Sulfur Oxidation and Contrail Precursor Chemistry

Kenneth J. De Witt
University of Toledo, Toledo, Ohio

Since its founding, NASA has been dedicated to the advancement of aeronautics and space science. The NASA Scientific and Technical Information (STI) Program Office plays a key part in helping NASA maintain this important role.

The NASA STI Program Office is operated by Langley Research Center, the Lead Center for NASA's scientific and technical information. The NASA STI Program Office provides access to the NASA STI Database, the largest collection of aeronautical and space science STI in the world. The Program Office is also NASA's institutional mechanism for disseminating the results of its research and development activities. These results are published by NASA in the NASA STI Report Series, which includes the following report types:

- TECHNICAL PUBLICATION. Reports of completed research or a major significant phase of research that present the results of NASA programs and include extensive data or theoretical analysis. Includes compilations of significant scientific and technical data and information deemed to be of continuing reference value. NASA's counterpart of peer-reviewed formal professional papers but has less stringent limitations on manuscript length and extent of graphic presentations.

- TECHNICAL MEMORANDUM. Scientific and technical findings that are preliminary or of specialized interest, e.g., quick release reports, working papers, and bibliographies that contain minimal annotation. Does not contain extensive analysis.

- CONTRACTOR REPORT. Scientific and technical findings by NASA-sponsored contractors and grantees.

- CONFERENCE PUBLICATION. Collected papers from scientific and technical conferences, symposia, seminars, or other meetings sponsored or cosponsored by NASA.

- SPECIAL PUBLICATION. Scientific, technical, or historical information from NASA programs, projects, and missions, often concerned with subjects having substantial public interest.

- TECHNICAL TRANSLATION. English-language translations of foreign scientific and technical material pertinent to NASA's mission.

Specialized services that complement the STI Program Office's diverse offerings include creating custom thesauri, building customized databases, organizing and publishing research results . . . even providing videos.

For more information about the NASA STI Program Office, see the following:

- Access the NASA STI Program Home Page at *http://www.sti.nasa.gov*

- E-mail your question via the Internet to help@sti.nasa.gov

- Fax your question to the NASA Access Help Desk at 301–621–0134

- Telephone the NASA Access Help Desk at 301–621–0390

- Write to:
  NASA Access Help Desk
  NASA Center for AeroSpace Information
  7121 Standard Drive
  Hanover, MD 21076

NASA/CR—2003-212293

Sulfur Oxidation and Contrail Precursor Chemistry

Kenneth J. De Witt
University of Toledo, Toledo, Ohio

National Aeronautics and
Space Administration

Glenn Research Center

April 2003

Acknowledgments

This report contains preliminary
findings, subject to revision as
analysis proceeds.

Sulfur Oxidation and Contrail Precursor Chemistry

Kenneth J. De Witt, Principal Investigator
Department of Chemical Engineering
The University of Toledo
Toledo, Ohio 43606

Abstract

Sulfuric acid (H_2SO_4), formed in commercial aircraft operations via fuel$-$S $\rightarrow$ SO_2 $\rightarrow$ SO_3 $\rightarrow$ H_2SO_4, plays an important role in the formation of contrails. It is believed that the first step occurs inside the combustor, the second step in the engine exit nozzle, and the third step in the exhaust plume. Thus, measurements of the sulfur oxidation rates are critical to the understanding of contrail formation. Field measurements of contrails formed behind commercial aircraft indicate that significantly greater conversion of fuel-bound sulfur to sulfate aerosol occurs than can be explained by our current knowledge of contrail physics and chemistry. The conversion of sulfur from S(IV) to S(VI) oxidation state, required for sulfate aerosol formation, is thermodynamically favored for the conditions that exist within jet engines but is kinetically disfavored. The principal reaction pathway is $O+SO_2+M$ $\rightarrow$ SO_3+M. The rates of this reaction have never been measured in the temperature and pressure regimes available to aircraft operation.

In the first year (FY02) of this project, we performed a series of experiments to elucidate the rate information for the $O+SO_2+M$ $\rightarrow$ SO_3+M reaction. The work performed is described below, following the proposed work plan. Because we used the H_2/O_2 system for an O-atom source and rate coefficients were obtained via computer simulation, construction of a reaction mechanism and either recalculation or estimation of thermodynamic properties of H_xSO_y species are described first.

Reaction Mechanism of the $SO_2/H_2/O_2$ System

For the H_2/O_2 system, we adopted a reaction mechanism of 20 elementary reactions that has been tested extensively at various conditions.[1-3] Then, additional reactions for SO_2 oxidation by H_xO_y species in the $SO_2/H_2/O_2$ system and their rate coefficients were critically reviewed and a reaction mechanism of 19 reactions for this system was composed. A comprehensive but truncated reaction mechanism for the $SO_2/H_2/O_2$ system is given in Table I of Appendix A. A brief review of important rate coefficients is given in the Discussion section.

Thermodynamic data of relevant species of $H_2/O_2/SO_2$ System

In computer modeling using a reaction mechanism for practical combustion systems or for extracting rate coefficient information, reliable thermodynamic properties ($\Delta_f H^0$(298.15 K), $H(T)$, $S(T)$, $G(T)$, $C_p(T)$) of the reacting species are necessary. Recently the value of $D^0_{298.15}$(H-OH)=118.81 ± 0.07 $kcal$ mol^{-1} was measured by Ruscic et al.[4] From this new bond dissociation

enthalpy of H_2O, Δ_fH^0(298.15 K) of OH=8.91 ± 0.07 $kcal\,mol^{-1}$ has been reestablished and the differences from the widely used value of Gurvich et al.[5] or JANAF[6] have been discussed in great detail.[4] Previously we had used 9.41 ± 0.05 $kcal\,mol^{-1}$ for Δ_fH^0(298.15 K) of OH, based upon the recommendation of Gurvich et al. The difference of 0.49 $kcal\,mol^{-1}$ from the new value of Ruscic et al. is quite large. Considering the uncertainty in obtaining D^0(O-H) by Gurvich et al. from spectroscopic measurements and an unambiguous direct measurement of D^0(H-OH) by a photoionization experiment by Ruscic et al., we adopted the new Δ_fH^0(298.15 K) of OH=8.91 ± 0.07 $kcal\,mol^{-1}$ of Ruscic et al. and readjusted all thermodynamic properties of OH accordingly. The thermodynamic properties of other species in the H_2/O_2 system are unchanged.

While thermodynamic properties of species in the H_2/O_2 system are more or less well established, those of H_xSO_y species (HS, HSO, HOSO, HSO_2, and $HOSO_2$) are virtually unknown. Using available experimental data and theoretical calculations, thermodynamic data of these species are estimated. Details are described in Appendix B.

Selection of Experimental Conditions via Sensitivity Analysis

In determining rate coefficients of the reaction

$$O+SO_2+M \rightarrow SO_3+M \qquad\qquad (R21)$$

an O-atom source must be found. In this work O-atoms were produced from H_2/O_2 reactions. I.e., the H_2/O_2 reaction system was perturbed with a small amount of SO_2. The major reactions that consume and produce O-atoms in the H_2/O_2 system are, respectively

$$O+H_2 \rightarrow OH+H \qquad\qquad (R2)$$
and
$$H+O_2 \rightarrow OH+O \qquad\qquad (R1)$$

Hence, in the $SO_2/H_2/O_2$ system, R21 would compete with R2. If we use rich H_2/O_2 mixtures, O-atoms would be consumed mainly by R2. This restricts us to consider lean H_2/O_2 mixtures only. Figure 1 shows $R=|\log([i]_{pk}/[H_2]_0)|$ as a function of equivalence ratio ϕ of H_2/O_2 mixtures, where i=O, OH, and H. Small R values indicate production of a large amount of species i. Obviously, lean mixtures are more suitable than rich mixtures in this regard. However, at given jet engine exhaust nozzle temperatures (900 to 1200 K), the following reaction will compete with R1 for H-atoms

$$H+O_2+M \rightarrow HO_2+M \qquad\qquad (R9)$$

Thus, it is also desirable to select reaction mixtures that produce a less amount of H-atoms.

Sensitivity analyses for an elapsed time to reach half of the absorption maximum (τ_{50}) were performed using the following baseline H_2/O_2 mixture (without SO_2) with various levels of sensitization by SO_2 at T=1000 K, ρ=15.0 $\mu mol\,cm^{-3}$; 0.5% H_2/10.0% O_2 (ϕ=0.025), 0.15%–3.0% SO_2/ 0.5% H_2/10.0% O_2 (ϕ=0.025)/Ar. In the baseline mixture, R9, R1, R2, and R3 show sensitivities for τ_{50} in that order. Figure 2(a) shows a sensitivity spectra for 0.5% H_2/10.0%

O_2/89.5% Ar mixture. Adding 0.15%, 0.25%, and 0.5% SO_2 to a 0.5% H_2/10.0% O_2/Ar mixture produced only a trace level of sensitivity for R21. The sensitivity of R21 was found to be dependent upon the SO_2/H_2 ratio in the mixture. Furthermore, as the SO_2/H_2 ratio is increased, the sensitivity of R21 and R9 is notably increased together with the relative importance of R21 over R9. Figure 2(b) shows a sensitivity spectra for the 2.0% SO_2/ 0.5% H_2/10.0% O_2/88.5% Ar mixture. Based upon this sensitivity analyses we selected the following three mixtures: for the baseline experiments, 0.5% H_2/10.0% O_2/89.5% Ar; for sensitization experiments, 2.0% SO_2/0.5% H_2/10.0% O_2/87.5% Ar and 3.0% SO_2/0.5% H_2/10.0% O_2/86.5% Ar.

Experimental

The shock tube-laser absorption technique is described in detail elsewhere.[3] Briefly, the test section of the shock tube was routinely pumped below $3\,\mu$ Torr by a Varian V60 Turbopump. The combined leak and out-gassing rate of the test section was $5\,\mu$ Torr min^{-1}. All shocks were initiated within 1 minute of admitting the test gas mixture. Shock velocities were measured using 4 flush-mounted 113A21 PCB Piezotronics pressure transducers coupled to Phillips PM6666 programmable counter-timers. The last pressure transducer was axially coincident with the center of the observation windows, 12.7 mm distant from the end wall. Shock speeds were fitted to a second-order polynomial in distance. The extrapolated speed to the end wall was used together with NASA thermodynamic data[7] in solving the standard relationships for the reflected shock properties, assuming full vibrational relaxation and no chemical reaction at the shock front. The computed reflected shock properties were corrected for boundary layer interaction effects using the similar method of Michael and Sutherland.[3,8,9]

The combined OH and SO_2 absorption profiles were measured at 310.032 nm (in air), corresponding to the P1(5) line of the (0,0) band of the OH $A^2\Sigma^+ \leftarrow X^2\Pi$ transition—at this wavelength, SO_2 also shows some absorption. The UV light was produced by a CW argon ion laser (Coherent Innova 200) pumped ring-dye laser (Coherent 899 - 21) running Kiton Red 620 dye. Intracavity frequency doubling was achieved with an angle tuned $LiIO_3$ crystal. For the detection of OH radicals and SO_2 molecules, a triple beam scheme was employed; probe beam, intensity reference beam and a wavelength reference beam (through a burner-stabilized methane/air flame). The detector was a combination of interference filter (310 nm with 10 nm fwhm)—PMT(Thorn EMI9924QB)—high speed buffer/amplifier. The S/N of the "probe beam-intensity reference beam" was usually better than 100. The overall electronic time constant determined for the entire PMT-buffer-cable system was less than $0.5\,\mu$ s.

H_2/O_2/Ar and SO_2/H_2/O_2/Ar test gas mixtures were prepared manometrically and allowed to stand for 48 hr before use. Gases were used without further purification. The stated purities were: H_2, 99.9995% (MG Industries, Scientific Grade); O_2, 99.998% (MG Industries, Scientific Grade); SO_2 (anhydrous), 99.98 wt.% (MG Industries, Scientific Grade); Ar, 99.9999% (MG Industries, Sputtering Grade).

Results

Because 310 nm UV light is also absorbed by SO_2 molecules, it is necessary to determine absorption coefficients of SO_2 ($\varepsilon_e(SO_2)$). The values of $\varepsilon_e(SO_2)$ determined are shown in Figure 3. A least squares fit to the data gives an expression

$$\varepsilon_e(SO_2) = 2.16 \times 10^5 \exp(-765.0 \text{ K/T}) \text{ cm}^2 \text{ mol}^{-1}$$

Evaluation of a characteristic time (τ_{50}) in the baseline experiments was done in the usual way. However, in the sensitization experiments, because there have always been long delays for sensible absorption signal rise (OH production), initial absorption by SO_2 immediately after the reflected shock was subtracted from the total absorption signal and τ_{50} values were evaluated as in the baseline experiments. Figure 4 shows τ_{50} values measured for the baseline mixture, 0.5% H_2/10.0% O_2/89.5% Ar, and for the sensitization mixtures, 2.0, 3.0% SO_2/0.5% H_2/10.0% O_2/86.5, 87.5% Ar. Throughout all of the experiments, densities were kept nearly the same between the baseline and sensitization experiments.

As seen in the figure, the τ_{50} values of sensitization mixtures are longer at low temperatures and increase with SO_2/H_2 ratio. At temperatures above 1200 K, the differences disappear between the two levels of sensitization.

Discussion

H_2/O_2 System

Because we generated O-atoms from the H_2/O_2 reaction system, a complete understanding of the H_2/O_2 reaction chemistry is a prerequisite for rate coefficient determination of the $O+SO_2+M \rightarrow SO_3+M$ reaction (R21). There are three key reactions in H_2/O_2 chemistry: chain branching $H+O_2 \rightarrow OH+O$ (R1), chain propagating $O+H_2 \rightarrow OH+H$ (R2) and chain terminating $H+O_2+M \rightarrow HO_2+M$ (R9). A comprehensive review of these three reactions is given here.

$$\text{(a) Chain Branching } H+O_2 \rightarrow OH+O \qquad \text{(R1)}$$

Figure A(1) in Appendix A shows the rate coefficient expressions reported recently. The current widely used rate coefficient expressions are those of Du and Hessler,[10] Baulch et al.[11] and GRI.[12] Du and Hessler obtained their k_1 expression, $k_1 = 9.76 \times 10^{13} \exp(-7474 \text{ K/T}) \text{ cm}^3 \text{ mol}^{-1} \text{ s}^{-1}$ (960 to 5300 K) by combining their rate coefficient measurements at very high temperatures (3450 to 5300 K) with the results of Masten et al.[13] (1450 to 3370 K), Shin and Michael[14] (1103 to 2055 K) and Pirraglia et al.[15] (962 to 1705 K). The compilation by Baulch et al. gives an expression identical to that of Du and Hessler. Pirraglia et al. combined their relatively low temperature results with the high temperature data of Frank and Just[16] (1693 to 2577 K) and reported $k_1 = 1.9 \times 10^{14} \exp(-8272 \text{ K/T}) \text{ cm}^3 \text{ mol}^{-1} \text{ s}^{-1}$ (962 to 2577 K). The GRI expression, $k_1 = 2.65 \times 10^{16} T^{-0.6707} \exp(-8575 \text{ K/T}) \text{ cm}^3 \text{ mol}^{-1} \text{ s}^{-1}$ (300 to 3000 K) is a fit to the combined high temperature results of Yu et al.[17] (which, in turn, the results of Yuan et al.[18] and of Masten et al.) and the somewhat low rate coefficients of Pirraglia et al. (especially low temperature data) with the room temperature data compiled by Demore et al.[19] Previously, we (GRC)[1] reported $k_1 = 7.13 \times 10^{13}$

exp(–6957 K/T) cm^{3}mol^{-1}s^{-1} (1050 to 2500 K) based upon OH radical growth rate that eliminates any H-atom producing contaminant effect.

Since the $\Delta_f H^0$(298.15 K) value of OH has been remeasured (see above), virtually all k_1 values must be reexamined. Hence, with the new thermodata of OH we reevaluated our existing data. The rederived expression is $k_1 = 3.74 \times 10^{15}$ T$^{-0.467}$ exp(–7758 K/T) cm^3 mol^{-1} s^{-1}. Extrapolation of this expression to room temperature gives about a factor of 2.5 higher than the value recommended by Demore et al. As seen, this expression has a negative temperature dependence of the A-factor. The temperature dependence of the A-factor has been given by several authors: –0.907 by Schott,[20] –0.927 by Yuan et al.,[18] –0.7 by Masten et al.[13] and –0.816 and +0.500 by theoretical calculations of Miller[21] and Miller and Garrett,[22] respectively.

Due to the difficulty in performing experiments at relatively low temperatures, no group has extended their temperature range wide enough to obtain a consistent set of experimental data. Instead, the results of Pirraglia et al. (960 to 1200 K) have been extensively used for the fit of the k_1 expression by various authors. Recently we measured OH absorption profiles in various H$_2$/O$_2$ systems at temperatures down to 950 K and up to 3500 K. We are currently analyzing these results. A combination of these new results with the previous ones reported in this laboratory[1] will form a consistent set of data over the widest temperature range (950 to 3500 K) ever employed by a single laboratory. Based upon this data set, a new rate coefficient expression will be produced and the validity of its temperature dependence of the A-factor and the extrapolated value to room temperature will be tested.

$$\text{(b) Chain Propagating O+H}_2 \rightarrow \text{OH+H} \qquad \qquad \text{(R2)}$$
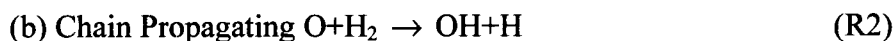
SO$_2$ molecules in the SO$_2$/H$_2$/O$_2$ system are consumed mainly by O+SO$_2$+M $\rightarrow$ SO$_3$+M (R21). The chain propagating reaction R2 inherently competes with R21 for O-atoms. Figure A(2) in Appendix A shows representative k_2 expressions published. Previously we presented $k_2 = 1.87 \times 10^{14}$ exp(–6854 K/T) cm^3 mol^{-1} s^{-1} (1420 to 2430 K). Reevaluation of OH absorption data obtained for k_2 evaluation with the new OH thermodata yielded $k_2 = 2.04 \times 10^{14}$ exp(–6972 K/T) cm^3 mol^{-1} s^{-1}. The differences between the old and new expressions are less than 3.5% in the given temperature range, the new expression being higher with temperature. One notable expression for k_2 is that of Sutherland et al.[23] Sutherland et al. reported a non-Arrhenius type rate coefficient expression, $k_2 = 5.06 \times 10^4$ T$^{2.67}$ exp(–3480 K/T) cm^3 mol^{-1} s^{-1} by combining their results of flash photolysis-shock tube work (880 to 2495 K) and the flash photolysis-resonance fluorescence technique (504 to 923 K) with the low temperature data of Presser and Gordon (297 to 471 K).[24] Our k_2 expression represents the high temperature data (880 to 2495 K) of Sutherland et al. quite well. However, due to the nature of a non-Arrhenius type curve fit, the extended temperature fit of Sutherland et al. over-predicts their results at temperatures around 950 K and above 2500 K. Therefore, in our temperature range (950 to 1100 K), extrapolation of our expression should be more appropriate.

$$\text{(c) Chain Terminating H+O}_2\text{+M} \rightarrow \text{HO}_2\text{+M} \qquad \qquad \text{(R9)}$$
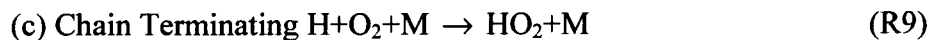
The chain terminating R9 reaction plays a governing role for ignition and flame characteristics at high pressure and especially at low temperature conditions (see sensitivity spectra in Figure 2).

For this reason, many authors[1, 25–42] investigated this reaction to determine rate coefficients. Experimental data and k_9 expressions are plotted in Figure A(3). At room temperature a consensus value has been established.[33] However, in the temperature range of combustion (T>750 K), the scatter of rate coefficient data is very large. For example, at T=~1000 K, there is a factor of 3 scatter in the k_9 values. We performed a series of experiments to determine the k_9 values in the temperature range of 950 to 1150 K using a shock tube—laser OH absorption spectroscopy technique in H_2/O_2 system. Experimental data were fit to $k_9=3.75\times10^{17}\ T^{-0.7}\ cm^6$ $mol^{-2}\ s^{-1}$. Our values positioned somewhat in the middle of the data scatter at T=~1000 K. Extrapolation of our k_9 expression also well represents the data of Hsu et al.[32] at temperatures between 296 K and 640 K and the room temperature result of Carleton et al.[33]

$SO_2/H_2/O_2$ System

As mentioned before, sensitization was used with 2% and 3% SO_2. Sensitization resulted in a remarkable increase of τ_{50} (see Figure 4). The effect of sensitization level on τ_{50} becomes more noticeable as temperature decreases, but it diminishes as temperature increases. Nevertheless, this increase of τ_{50} is due to depletion of O-atoms by R21, so the H-atom production rate by R2 is reduced. This, in turn, reduces the branching rate of R1.

The rate coefficients of R21 are derived by computer simulation using the Table I mechanism in Appendix A. In computer simulation, at each experimental condition, only the starting k_{21} value was varied so as to minimize the difference between the computed and experimental τ_{50}. Figure 5 shows the provisional k_{21} values obtained in this work. R21 is a pressure (density) dependent reaction. For this type of reaction, it is usual to use two rate coefficient expressions at the extreme conditions, a low pressure limit $k_{21,0}$ and a high pressure limit $k_{21,\infty}$. The rate coefficients in the fall-off region are then obtained by interpolation using these two extreme rate coefficients. Obviously R21 is in the falloff region in our experimental conditions. Therefore we computed the starting k_{21} value using the $k_{21,0}$, $k_{21,\infty}$, and a simple Lindemann-Hinshelwood interpolation formula

$$k_{21}/k_{21,\infty}=(k_{21,0}/k_{21,\infty})/(1+k_{21,0}/k_{21,\infty})=x/(1+x)$$

where $x=k_{21,0}/k_{21,\infty}$.

For $k_{21,\infty}$ and $k_{21,0}$ we used the expressions given by Mueller et al.,[43] $k_{21,\infty}=9.2\times10^{10}\ exp(-1200\ K/T)\ cm^3\ mol^{-1}\ s^{-1}$ and by Troe,[44] $k_{21,0}=4.0\times10^{28}\ T^{-4.0}\ exp(-2650\ K/T)\ cm^6\ mol^{-2}\ s^{-1}$, respectively. The $k_{21,\infty}$ of Mueller et al. is the only high pressure limit expression ever reported. Several measurements of $k_{21,0}$ have been reported either at high temperatures[45,46] (1435 to 2500 K) or at low temperatures (<430 K).[19,47–50] In the temperature range of our interest (900 to 1100 K), no experimental measurements are available. The $k_{21,0}$ expression shown above was made by Troe by fitting the low and high temperature data. Note that at T<500 K, the rate coefficient value increases with temperature (positive activation energy), while at T>500 K, it decreases with temperature (negative activation energy). Our provisional k_{21} values obtained in the falloff region are about a factor of 2 to 3 higher than the theoretical calculations using the equation shown above.

Conclusions

Existing data for H_2/O_2 and $SO_2/H_2/O_2$ chemistry were critically reviewed and a reaction mechanism was assembled (Table I in Appendix A). Optimum $H_2/O_2/Ar$ and $SO_2/H_2/O_2/Ar$ mixture compositions and experimental conditions were established via a series of sensitivity analyses. Shock tube experiments were performed using OH laser absorption spectroscopy for the $H_2/O_2/Ar$ mixtures to examine baseline behavior and for the $SO_2/H_2/O_2/Ar$ mixtures to determine k_{21} values for the conditions selected. The experimental results were analyzed via computer simulations and the provisional rate coefficients of R21 were obtained. The provisional rate coefficients of R21 (k_{21} values) obtained in our experimental conditions are about a factor of 2 to 3 higher than the theoretical calculations using the expressions of $k_{21,0}$, $k_{21,\infty}$, and the parameters of the interpolation formula in Table I of Appendix A. Additionally, temperature dependent absorption coefficients of SO_2 at OH absorption wavelength were measured.

Measured or calculated thermochemical and structural data for HS, HSO, HOSO, HSO_2, and $HOSO_2$ species were critically reviewed and thermodynamic data for these species were obtained (Appendix B).

Future Work

In the second year of this project, besides what is contained in the project plan, the collision efficiency effect of SO_2 the on pressure dependent reactions, R9 and R21, and the interpolation formula used in determination of k_{21} will be examined further. In pressure dependent reactions, reaction rates increase with pressure. The increase of collision efficiencies of collision partners is equivalent to an increase of density (pressure). If one assigns a high collision efficiency of SO_2 to R9 and R21, their reaction rates and τ_{50} values will increase and result in a lowering of k_{21} values. (Currently we used a collision efficiency of 1 for SO_2 for R9 and R21.) Experiments at various densities will also be performed to optimize the falloff parameters. Data analysis will be completed for the experiments performed to determine the rate coefficients of the chain branching reaction R1.

References

1.   Ryu, Si-OK; Hwang, Soon Muk; Rabinowitz, Martin Jay; *J. Phys. Chem.* 1995, *99*, 13984.
2.   Ryu, Si-Ok; Hwang, Soon Muk; Rabinowitz, Martin Jay; *Chem. Phys. Lett.* 1995, *242*, 279.
3.   Hwang, S. M.; Ryu, Si-OK; De Witt, K. J.; Rabinowitz, M. J.; *J. Phys. Chem. A* 1999, *103*, 5949.
4.   Ruscic, B; Wagner, Albert F.; Harding, L. B.; Asher, R. L.; Feller, D.; Dixon, D. A.; Peterson, K. A.; Song, Y.; Qian, X.; Ng, C.-Y.; Liu, J.; Chen, W.; Schwenke, D. W.; *J. Phys. Chem. A* 2002, *106*, 2727.
5.   Gurvich, L. V.; Veyts, I. V.; Alcock, C. B.; "Thermodynamic Properties of Individual Substances." Vol. 1, parts 1 and 2; Hemisphere Publishing Corp.: New York, 1989.
6.   Chase, M. W., Jr.; Davis, C. A.; Downey, J. R.; Frurip, D. J.; McDonald, R. A.; Syverud, A. N.; *J. Phys. Chem. Ref. Data* 1985, *14*, Suppl. 1.

7. McBride, B. J.; Zehe, M. J.; Gordon, S.; "NASA Glenn Coefficients for Calculating Thermodynamic Properties of Individual Species." NASA/TP-2002-211556; NASA Glenn Research Center: September 2002.

8. Michael, J. V.; Sutherland, J. W.; *Int. J. Chem. Kinet.* 1986, *18*, 409.

9. Hwang, S. M.; Ryu, Si-OK; De Witt, K. J.; Rabinowitz, M. J.; *J. Phys. Chem. A* 2000, *104*, 9803.

10. Du, H.; Hessler, J. P.; *J. Chem. Phys.* 1992, *96*, 1077.

11. Baulch, D. L.; Cobos, C. J.; Cox, R. A.; Frank, P.; Hayman, G.; Just, Th.; Kerr, J. A.; Murrells, T.; Pilling, M. J.; Troe, J.; Walker, R. W.; Warnatz, J.; *J. Phys. Chem. Ref. Data* 1994, *23*, 847.

12. Smith, G. P.; Golden, D. M.; Frenklach, M.; Moriaty, N. W.; Eiteneer, B.; Goldenberg, M.; Bowman, C. T.; Hanson, R. K.; Song, S.; Gardiner, W. C., Jr.; Lissianski, V. V.; Qin, Z.; http://www.me.berkeley.edu/gri_mech/

13. Masten, D. A.; Hanson, R. K.; Bowman, C. T.; *J. Phys. Chem.* 1990, *94*, 7119.

14. Shin, K. S.; Michael, J. V.; *J. Chem. Phys.* 1991, *95*, 262.

15. Pirraglia, A. N.; Michael, J. V.; Sutherland, J. W.; Klemm, R. B.; *J. Phys. Chem.* 1989, *93*, 282.

16. Frank, P.; Just, *Th. Ber. Busen-Ges. Phys. Chem.* 1985, *89*, 181.

17. Yu, C.-L.; Frenklach, M.; Masten, D. A.; Hanson, R. K.; Bowman, C. T.; *J. Phys. Chem.* 1994, *98*, 4770.

18. Yuan, T.; Wang, C.; Yu, C.-L.; Frenklach, M.; Rabinowitz, M.; J. *J. Phys. Chem.* 1991, *95*, 1258.

19. DeMore, W. B.; Sander, S. P.; Golden, D. M.; Hampson, R. F.; Kurylo, M. J.; Howard, C. J.; Ravishankara, A. R.; Kolb, C. E.; Molina, M. J.; *Chemical Kinetics and Photochemical Data for use in Stratospheric Modeling*; Evaluation No. 12; JPL Publication 97-4; JPL: Pasadena, CA, January 15, 1997.

20. Schott, G. L.; *Combust Flame* 1973, *21*, 357.

21. Miller, J. A.; *J. Chem. Phys.* 1986, *84*, 6170.

22. Miller, J. A.; Garrett, B. C.; *Int. J. Chem. Kinet.* 1997, *29*, 275.

23. Sutherland, J. W.; Michael, J. V.; Pirraglia, A. N.; Nesbitt, F. L.; Klemm, R. B.; *Twenty-first Symposium (International) on Combustion*; The Combustion Institute: Pittsburgh, PA, 1986; p 929.

24. Presser, N.; Gordon, R. J.; *J. Chem. Phys.* 1985, *82*, 1291.

25. Getzinger, R. W.; Schott, G. L.; *J. Chem. Phys.* 1965, *43*, 3237.

26. Getzinger, R. W.; Blair, L. S.; *Combust. Flame* 1970, *14*, 5.

27. Gutman, D.; Hardwidge, E. A.; Dougherty, F. A.; Lutz, R. W.; *J. Chem. Phys.* 1967, *47*, 5950.

28. Pirraglia, A. N.; Michael, J. V.; Sutherland, J. W.; Klemm, R. B.; *J. Phys. Chem.* 1989, *93*, 282.

29. Davidson, D. F.; Petersen, E. L.; Röhrig, M.; Hanson, R. K.; Bowman, C. T.; *Twenty-Sixth Symposium (International) on Combustion*; The Combustion Institute: Pittsburgh, PA, 1996; p 481.

30. Ashman, P. J.; Haynes, B. S.; *Twenty-Seventh Symposium (International) on Combustion*; The Combustion Institute: Pittsburgh, PA, 1998; p 185.

31. Mueller, M. A.; Kim, T. J.; Yetter, R. A.; Dryer, F. L.; *Int. J. Chem. Kinet.* 1999, *31*, 113.

32. Hsu, K.-J.; Anderson, S. M.; Durant, J. L.; Kaufman, F.; *J. Phys. Chem.* 1989, *93*, 1018.

33. Carleton, K. L.; Kessler, W. J.; Marinelli, W.; *J. Phys. Chem.* 1993, *97*, 6412.
34. Kurylo, M. J.; *J. Phys. Chem.* 1972, *76*, 3518.
35. Wong, W.; Davis, D. D.; *Int. J. Chem. Kinet.* 1974, *1*, 401.
36. Cobos, C. J.; Hippler, H.; Troe, J.; *J. Phys. Chem.* 1985, *89*, 342.
37. Clyne, M. A. A.; Thrush, B. A.; *Proc. Roy. Soc. (London)* 1963, *A275*, 559.
38. Hikida, T.; Eyre, J. A.; Dorfman, L. M.; *J. Chem. Phys.* 1971, *54*, 3422.
39. Westenberg, A. A.; deHaas, N.; *J. Phys. Chem.* 1972, *76*, 1586.
40. Ahumada, J. J.; Michael, J. V.; Osborne, D. T.; *J. Chem. Phys.* 1972, *57*, 3736.
41. Bates, R. W.; Golden, D. M.; Hanson, R. K.; Bowman, C. T.; *Phys. Chem. Chem. Phys.* 2001, *3*, 2337.
42. Michael, J. V.; Su, M.-C.; Sutherland, J. W.; Carroll, J. J.; Wagner, A. F.; *J. Phys. Chem. A* 2002, *106*, 5297.
43. Mueller, M. A.; Yetter, R. A.; Dryer, F. L.; *Int. J. Chem. Kinet.* 2000, *32*, 317.
44. Troe, J.; *Ann. Rev. Phys. Chem.* 1978, *29*, 223.
45. Ashtoltz, D. C.; Glanzer, K.; Troe, J.; *J. Chem. Phys.* 1979, *70*, 2409.
46. Smith, O. I.; Tseregounis, S.; Wang, S.-N.; *Int. J. Chem. Kinet.* 1982, *14*, 679.
47. Atkinson, R.; Pitts, J. N., Jr.; *Int. J. Chem. Kinet.* 1978, *10*, 1081.
48. Mulcahy, M. F. R.; Steven, J. R.; Ward, J. C.; *J. Phys. Chem.* 1967, *71*, 2124.
49. Westenberg, A. A.; deHaas, N.; *J. Chem. Phys.* 1975, *63*, 5411.
50. Atkinson, R,; Baulch, D. L.; Cox, R. A.; Frank, P.; Hampson, R. F.; Kerr, J. A.; Rossi, M. J.; Troe, J.; *J. Phys. Chem. Ref. Data* 1997, *26*, 1329.
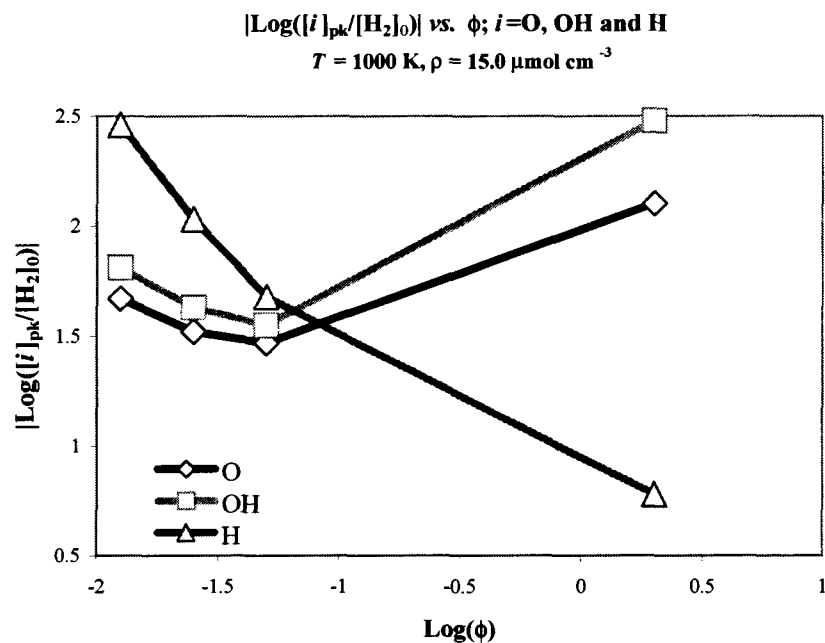
$|Log([i]_{pk}/[H_2]_0)|$ vs. ϕ; i =O, OH and H

$T = 1000$ K, $\rho = 15.0$ μmol cm^{-3}

2.5

2

$|Log([i]_{pk}/[H_2]_0)|$

1.5

1

◇ O
□ OH
△ H

0.5

-2   -1.5   -1   -0.5   0   0.5   1

$Log(\phi)$

Figure 1.—Absolute ratios of the peak concentrations of O- and H-atoms and OH radicals to the initial concentration of H_2 in the H_2/O_2/Ar mixtures as a function of the mixture equivalence ratio, ϕ, evaluated at T=1000 K and ρ =15.0 μ mol cm^{-3}. Large values indicate the suppression of peak concentrations.

0.5% H_2, 10.0% O_2, 89.5% Ar

T=1000 K, ρ=15.0 μmol cm^{-3}

$H_2+O_2+M=HO_2+M$

$OH+H_2=H_2O+H$

$O+H_2=OH+H$

$H+O_2=OH+O$

-1   -0.5   0   0.5   1   1.5
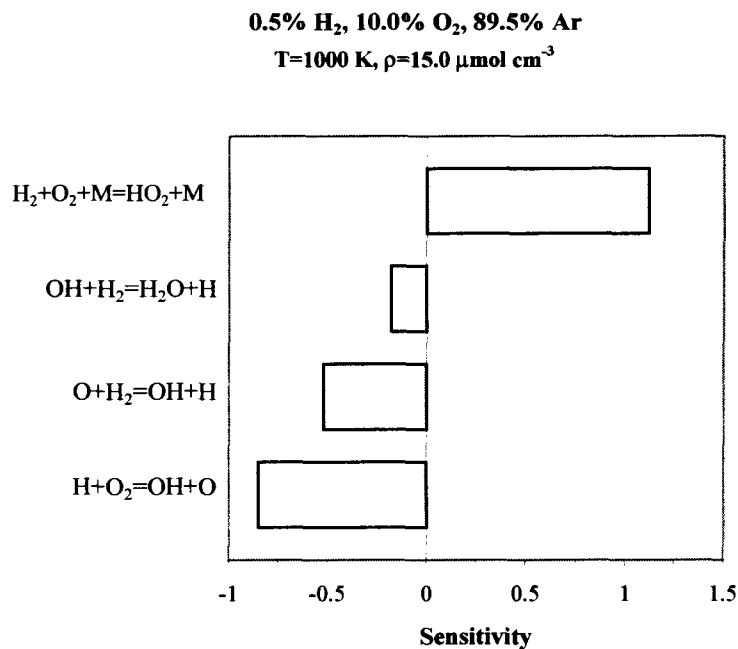
Sensitivity

Figure 2(a).—Sensitivity spectra for τ_{50} of the baseline mixture, 0.5% H_2/10.0% O_2/89.5% Ar. T=1000 K and ρ =15.0 μ mol cm^{-3}.

2.0% SO$_2$, 0.5% H$_2$, 10.0% O$_2$, 87.5% Ar

T=1000 K, ρ=15.0 μmol cm^{-3}
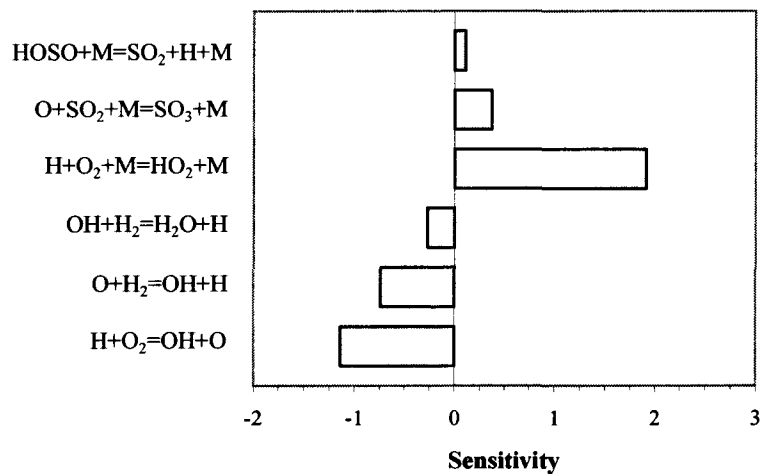
Figure 2(b).—Sensitivity spectra for τ_{50} of the 2.0% SO$_2$/0.5% H$_2$/10.0% O$_2$/87.5% Ar. T=1000 K and ρ =15.0 μ mol cm^{-3}.

Absorption Coefficients of SO$_2$ at 310 nm

$\varepsilon_e(SO_2)$=2.16 x 10^5 exp(-765.0 K/T) cm^2 mol^{-1}
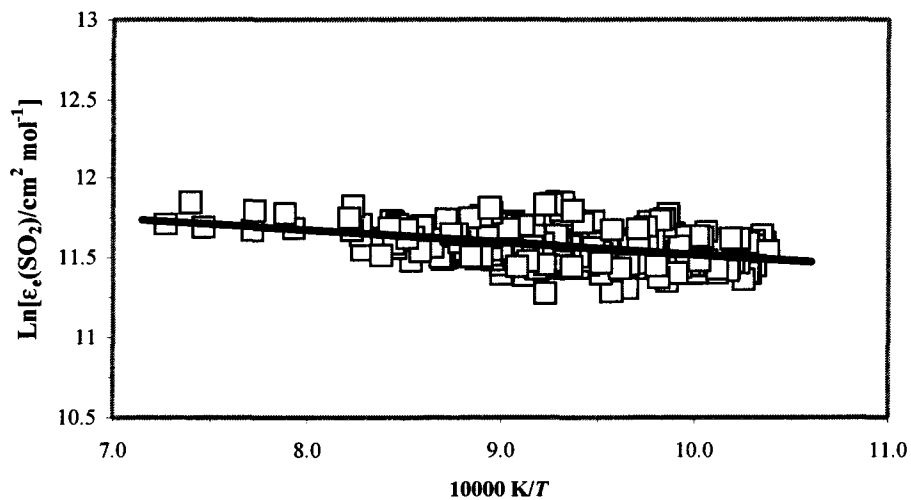
Figure 3.—Base 'e' absorption coefficients of SO$_2$ at 310 nm. The least squares fit expression is $\varepsilon_e(SO_2)$=2.16×10^5 exp(–765.0/T) cm^2 mol^{-1}.

SO₂/H₂/O₂/Ar
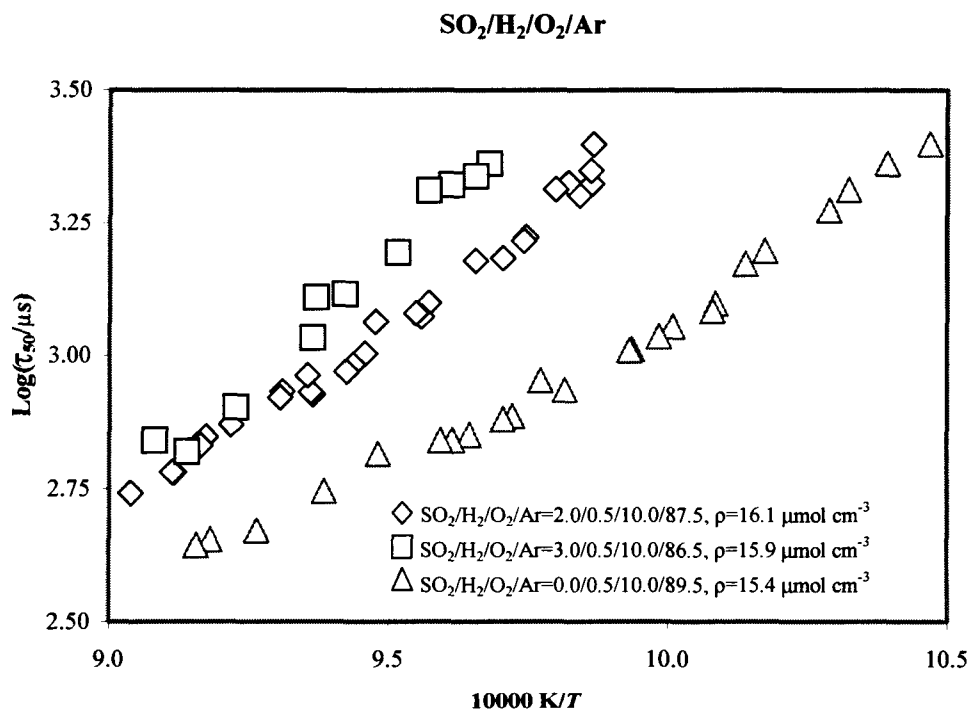
Figure 4.—Measured τ_{50} values of the baseline mixture, 0.5% H_2/10.0% O_2/89.5% Ar and two sensitization mixtures, 2.0% SO_2/0.5% H_2/10.0% O_2/87.5% Ar and 3.0% SO_2/0.5% H_2/10.0% O_2/86.5% Ar.
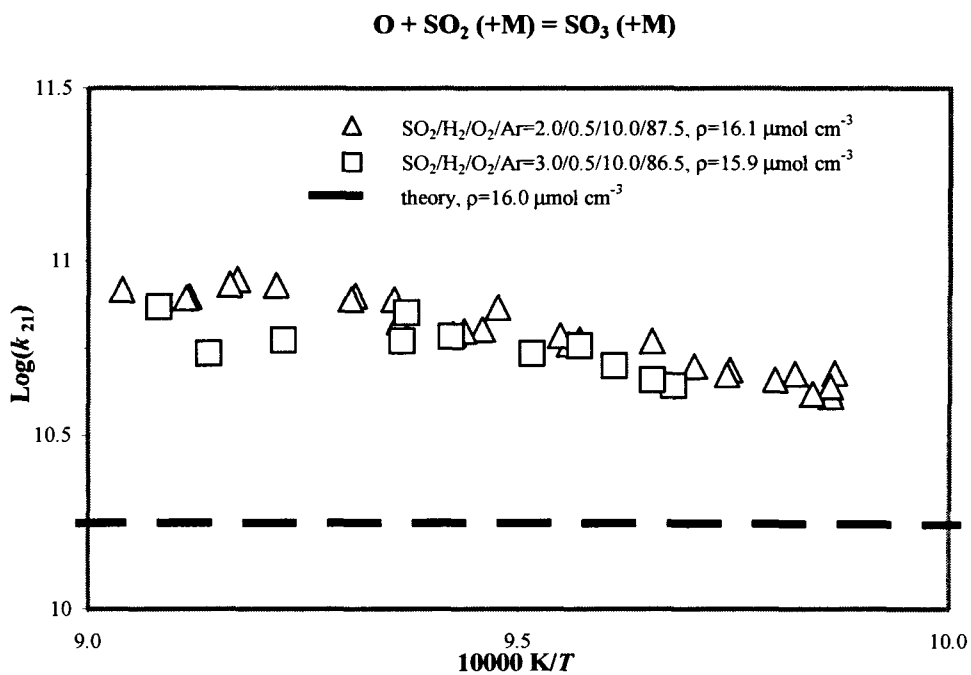
$O + SO_2 (+M) = SO_3 (+M)$

Figure 5.—The falloff k_{21} values of the reaction R21, $O+SO_2(+M) \rightarrow SO_3(+M)$.

Appendix A

Table I.—Reaction Mechanism[a]

	reaction	A	n	Θ	Note
1	$H+O_2=OH+O$	7.13E+13	0.0	6957	
2	$O+H_2=OH+H$	1.87E+14	0.0	6854	
3	$OH+H_2=H+H_2O$	2.16E+08	1.51	1726	
4	$O+H_2O=OH+OH$	4.51E+04	2.70	732	
5	$O+O+M=O_2+M$	1.0E+17	−1.0	0	
	Ar,1.0/ H_2,2.9/ O_2,1.2/ H_2O,18.5/				e
6	$H+H+M=H_2+M$	6.4E+17	−1.0	0	
	Ar,1.0/ H_2,4.0/ H_2O,12.0/ H,26.0/				e
7	$H+O+M=OH+M$	6.2E+16	−0.6	0	
	Ar,1.0/ H_2O,5.0/				e
8	$H+OH+M=H_2O+M$	8.4E+21	−2.0	0	
	Ar,1.0/ H_2,2.5/ H_2O,16.25/				e
9	$H+O_2+M=HO_2+M$	7.55E+17	−0.8	0	
	Ar,1.0/ O_2,1.33/ H_2,3.33/ H_2O,21.3/				e
10	$HO_2+H=OH+OH$	1.5E+14	0.0	505	
11	$HO_2+H=H_2+O_2$	2.5E+13	0.0	350	
12	$HO_2+H=H_2O+O$	5.0E+12	0.0	710	
13	$HO_2+O=O_2+OH$	2.0E+13	0.0	0	
14	$HO_2+OH=H_2O+O_2$	2.0E+13	0.0	0	
15	$HO_2+HO_2=O_2+H_2O_2$	1.3E+11	0.0	−820	f
	$HO_2+HO_2=O_2+H_2O_2$	4.2E+14	0.0	6039	f
16	$H_2O_2+M=OH+OH+M$	1.2E+17	0.0	22900	
	Ar,0.67/ O_2,0.78 / H_2O,6.0/				e
17	$H_2O_2+H=HO_2+H_2$	1.7E+12	0.0	1900	
18	$H_2O_2+H=H_2O+OH$	1.0E+13	0.0	1805	
19	$H_2O_2+O=HO_2+OH$	2.8E+13	0.0	3225	
20	$H_2O_2+OH=HO_2+H2O$	7.0E+12	0.0	720	
21	$SO_2+O+M=SO_3+M$	9.2E+10	0.0	1198	b
		4.0E+28	−4.0	2642	c
	1.000	1.000	0.0	0	d
	Ar,1.0/ O_2,1.33/ SO_2,1.0/				e
22	$SO_2+OH+M=HOSO_2+M$	7.2E+12	0.0	360	b
		4.5E+25	−3.3	360	c
	0.640	∞	300.0	0	d
	Ar,1.0/ O_2,1.5/ SO_2,12.1/[e]				e
23	$HOSO+M=SO_2+H+M$	1.7E+10	0.8	23602	b
		1.6E+31	−4.53	24759	c
	0.450	0.0	∞	∞	d
	Ar,0.75/ H_2,2.5/ H_2O,12.0/				e
24	$SO_2+OH=SO_3+H$	4.9E+02	2.69	11977	

Table I.—Reaction Mechanism^a (continued)

	reaction	A	n	Θ	Note
25	SO+O+M=SO$_2$+M	3.2E+13	0.0	0	b
		2.9E+24	−2.9	0	c
	0.550	0.0	∞	∞	d
	Ar,1.00/ O$_2$,1.33/ H$_2$O,10.0/				e
26	SO$_3$+O=SO$_2$+O$_2$	4.11E+11	0.0	3070	
27	SO$_3$+SO=SO$_2$+SO$_2$	1.0E+12	0.0	2013	
28	SO$_3$+H$_2$O=H$_2$SO$_4$	7.23E+08	0.0	0	
29	SO+OH+M=HOSO+M	8.0E+21	−2.16	418	
	Ar,0.75/ H$_2$,2.5/ H$_2$O,12.0/				e
30	SO+OH=SO$_2$+H	5.2E+13	0.0	0	
31	SO+O$_2$=SO$_2$+O	6.2E+03	2.42	1535	
32	HOSO+H=SO+H$_2$O	6.3E−10	6.29	−956	
33	HOSO+OH=SO$_2$+H$_2$O	1.0E+12	0.0	0	
34	HOSO+O$_2$=SO$_2$+HO$_2$	1.0E+12	0.0	503	
35	HOSO$_2$+M=SO$_3$+H+M	3.2E+16	−0.81	27024	
	Ar,0.75/ H$_2$,2.5/ H$_2$O,12.0/				e
36	HOSO$_2$+H=SO$_2$+H$_2$O	1.0E+12	0.0	0	
37	HOSO$_2$+O=SO$_3$+OH	5.0E+12	0.0	0	
38	HOSO$_2$+OH=SO$_3$+H$_2$O	1.0E+12	0.0	0	
39	HOSO$_2$+O$_2$=SO$_3$+HO$_2$	7.8E+11	0.0	330	

^{a} Rate coefficients are in the form, $k = AT^n \exp(-\Theta/T)$. Units are K, cm, mol, and s.

^{b} k_∞

^{c} k_0

^{d} Falloff correction parameters.
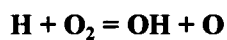
^{e} Collision efficiencies.

^{f} Duplicated reaction.
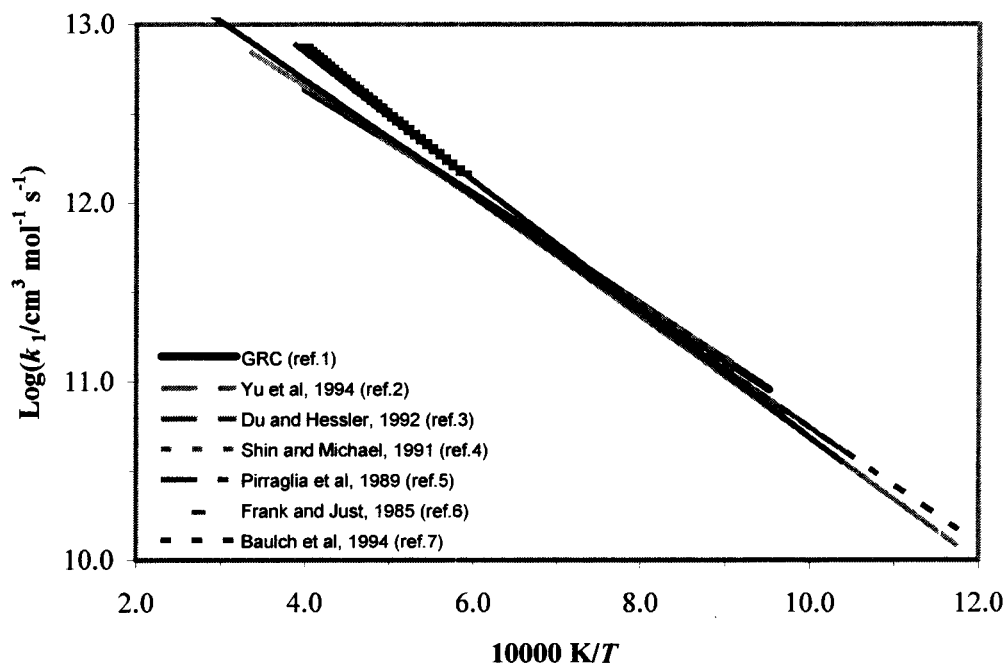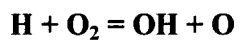
$$H + O_2 = OH + O$$

Figure A1(a).—Rate coefficients of R1, H+O$_2$ $\rightarrow$ OH+O.

$$H + O_2 = OH + O$$
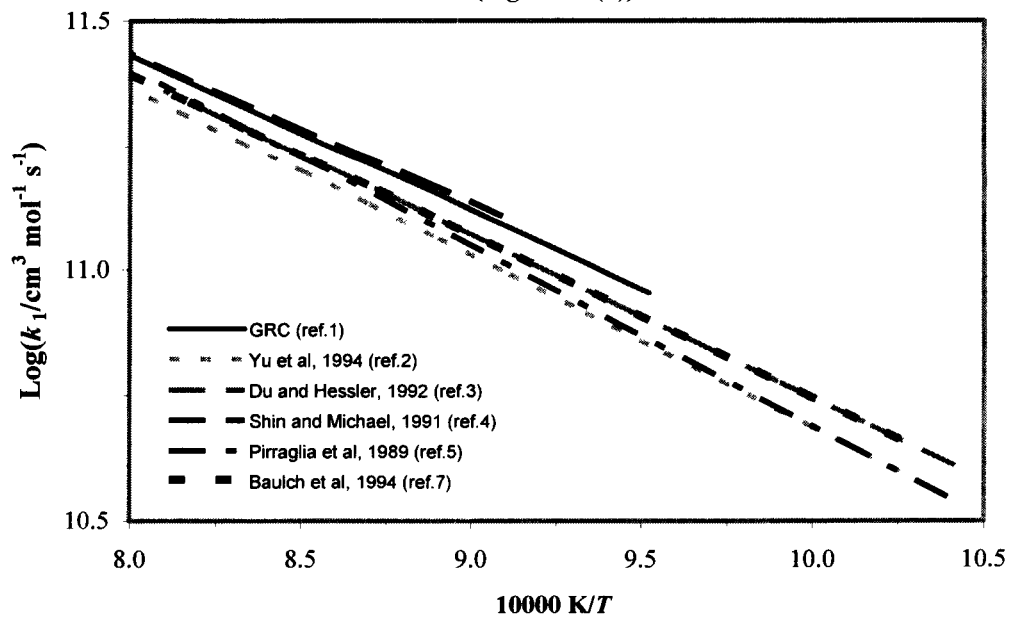(Figure A1(b))

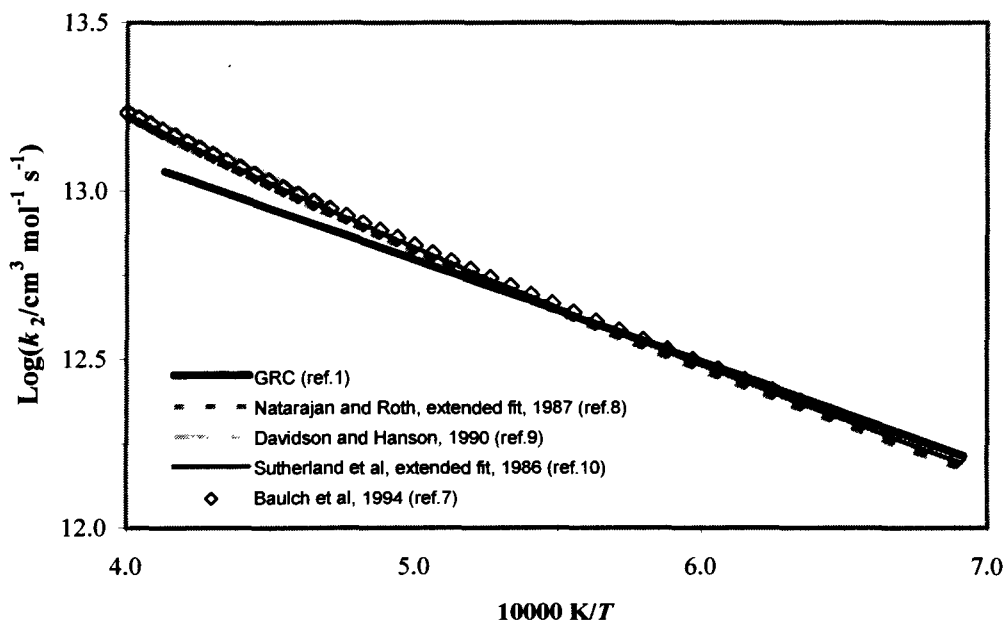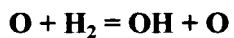Figure A1(b).—Exploded plot of the Figure A1(a) for the temperature range of 950 to 1250 K.

O + H$_2$ = OH + O

Figure A2(a).—Rate coefficients of R2, O+H$_2$ $\rightarrow$ OH+H.

O + H$_2$ = OH + O
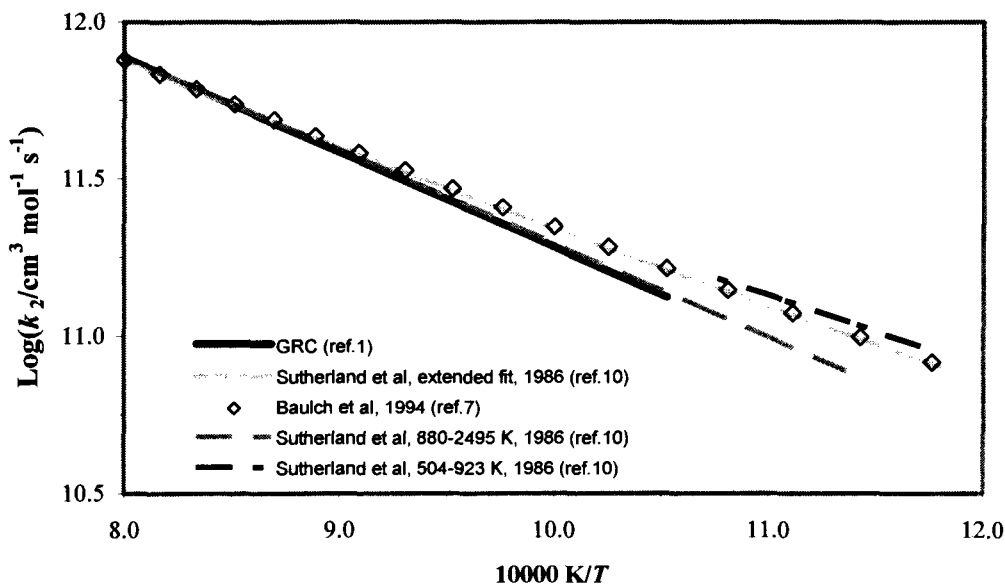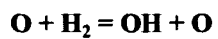
Figure A2(b).—Exploded plot of the Figure A2(a) for the temperature range of 830 to 1250 K.
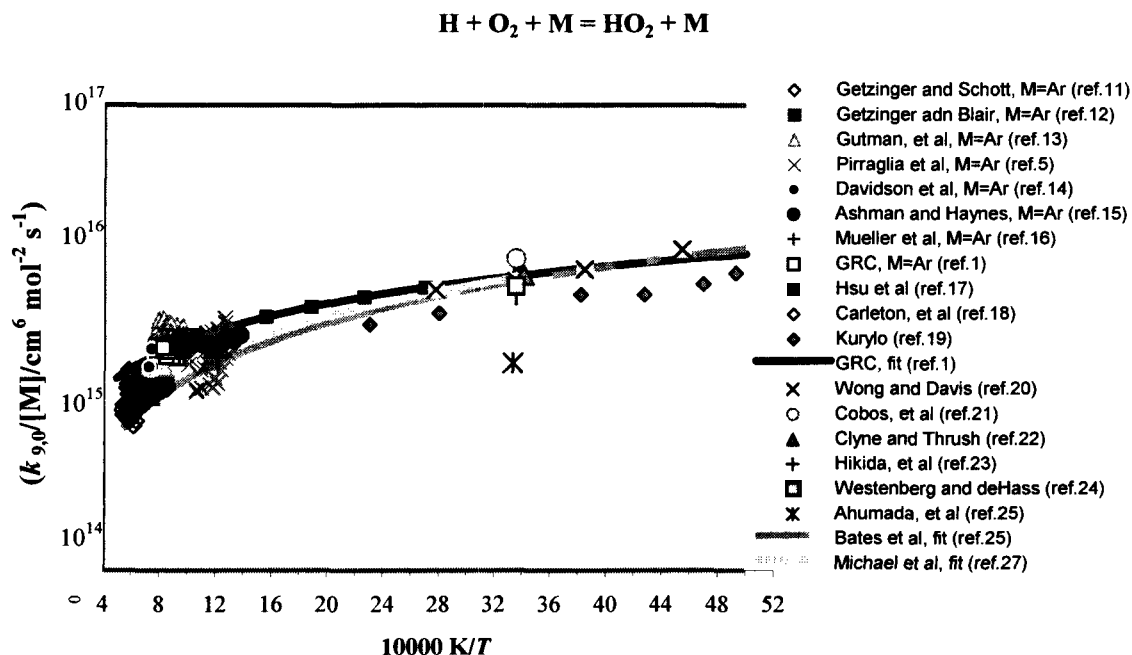
$$H + O_2 + M = HO_2 + M$$

Figure A3.—Rate coefficients of R9, $H+O_2+M \rightarrow HO_2+M$.
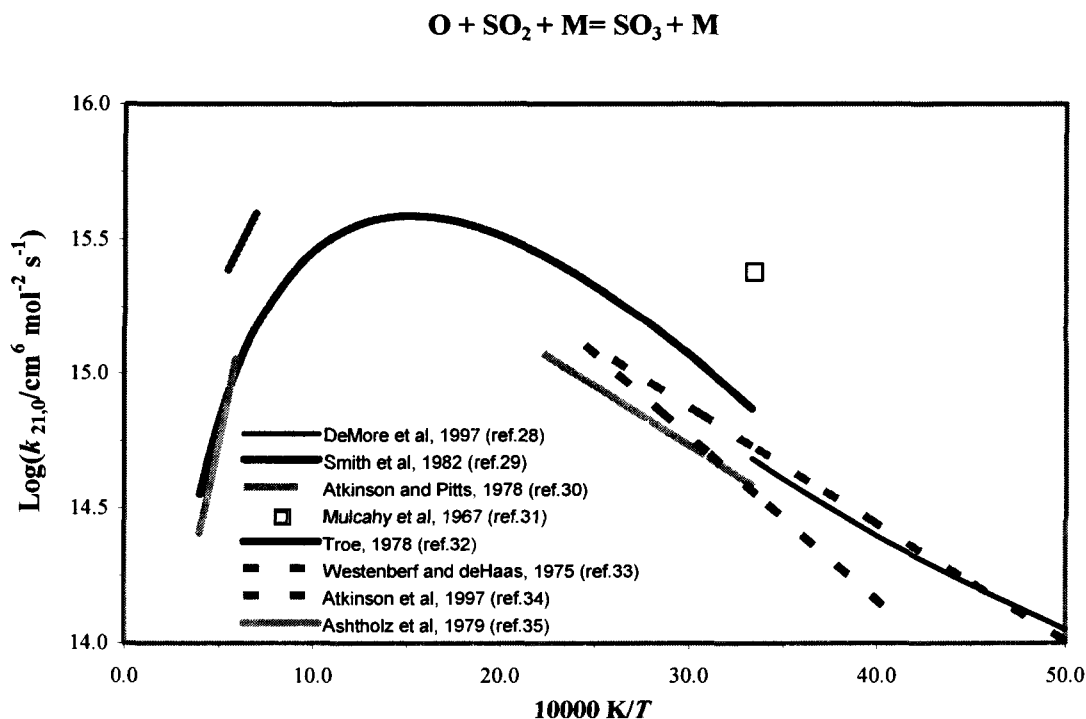
$$O + SO_2 + M = SO_3 + M$$

Figure A4(a).—Low pressure limit rate coefficients ($k_{21,0}$) of R21, $O+SO_2+M \rightarrow SO_3+M$.
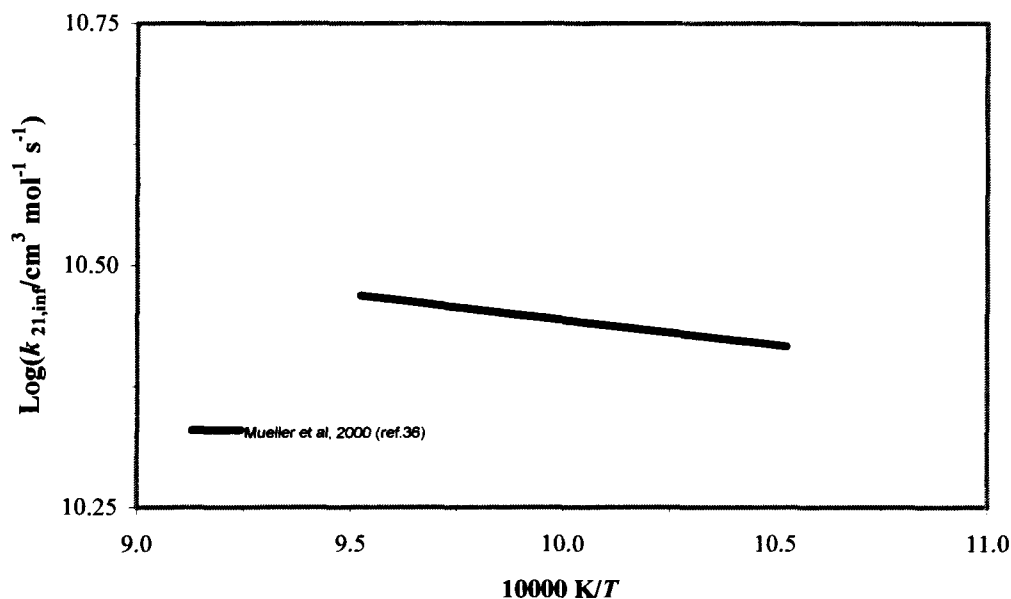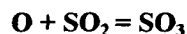
$$O + SO_2 = SO_3$$

Figure A4(b).—High pressure limit rate coefficients ($k_{21, \infty}$) of R21, O+SO$_2$ → SO$_3$.

References

1. Hwang, S. M.; De Witt, K. J.; Rabinowitz, M. J.; *This work* 2002
2. Yu, C.-L.; Frenklach, M.; Masten, D. A.; Hanson, R. K.; Bowman, C. T.; *J. Phys. Chem.* 1994, *98*, 4770.
3. Du, H.; Hessler; J. P.; *J. Chem. Phys.* 1992, *96*, 1077.
4. Shin, K. S.; Michael, J. V.; *J. Chem. Phys.* 1991, *95*, 262.
5. Pirraglia, A. N.; Michael, J. V.; Sutherland, J. W.; Klemm, R. B.; *J. Phys. Chem.* 1989, *93*, 282.
6. Baulch, D. L.; Cobos, C. J.; Cox, R. A.; Frank, P.; Hayman, G.; Just, Th.; Kerr, J. A.; Murrells, T.; Pilling, M. J.; Troe, J.; Walker, R. W.; Warnatz, J.; *J. Phys. Chem. Ref. Data* 1994, *23*, 847.
7. Frank, P.; Just, Th. *Ber. Busen-Ges. Phys. Chem.* 1985, *89*, 181.
8. Natarajan, K; Roth, P.; *Combust. Flame* 1987, *70*, 267.
9. Davidson, D. F.; Hanson, R. K.; *Combust. Flame* 1990, *82*, 445.
10. Sutherland, J. W.; Michael, J. V.; Pirraglia, A. N.; Nesbitt, F. L.; Klemm, R. B.; *Twenty-first Symposium (International) on Combustion*; The Combustion Institute: Pittsburgh, PA, 1986; p 929.
11. Getzinger, R. W.; Schott, G. L.; *J. Chem. Phys.* 1965, *43*, 3237.
12. Getzinger, R. W.; Blair, L. S.; *Combust. Flame* 1970, *14*, 5.
13. Gutman, D.; Hardwidge, E. A.; Dougherty, F. A.; Lutz, R. W.; *J. Chem. Phys.* 1967, *47*, 5950.

14. Davidson, D. F.; Petersen, E. L.; Röhrig, M.; Hanson, R. K.; Bowman, C. T.; *Twenty-Sixth Symposium (International) on Combustion*; The Combustion Institute: Pittsburgh, PA, 1996; p 481.

15. Ashman, P. J.; Haynes, B. S.; *Twenty-Seventh Symposium (International) on Combustion*; The Combustion Institute: Pittsburgh, PA, 1998; p 185.

16. Mueller, M. A.; Yetter, R. A.; Dryer, F. L.; *Twenty-Seventh Symposium (International) on Combustion*; The Combustion Institute: Pittsburgh, PA, 1998; p 177.

17. Hsu, K. -J.; Anderson, S. M.; Durant, J. L.; Kaufman, F.; *J. Phys. Chem.* 1989, *93*, 1018.

18. Carleton, K. L.; Kessler, W. J.; Marinelli, W.; *J. Phys. Chem.* 1993, *97*, 6412.

19. Kurylo, M. J.; *J. Phys. Chem.* 1972, *76*, 3518.

20. Wong, W.; Davis, D. D.; *Int. J. Chem. Kinet.* 1974, *1*, 401.

21. Cobos, C. J.; Hippler, H.; Troe, J.; *J. Phys. Chem.* 1985, *89*, 342.

22. Clyne, M. A. A.; Thrush, B. A.; *Proc. Roy. Soc. (London)* 1963, *A275*, 559.

23. Hikida, T.; Eyre, J. A.; Dorfman, L. M.; *J. Chem. Phys.* 1971, *54*, 3422.

24. Westenberg, A. A.; deHaas, N.; *J. Phys. Chem.* 1972, *76*, 1586.

25. Ahumada, J. J.; Michael, J. V.; Osborne, D. T.; *J. Chem. Phys.* 1972, *57*, 3736.

26. Bates, R. W.; Golden, D. M.; Hanson, R. K.; Bowman, C. T.; *Phys. Chem. Chem. Phys.* 2001, *3*, 2337.

27. Michael, J. V.; Su, M.-C.; Sutherland, J. W.; Carroll, J. J.; Wagner, A. F.; *J. Phys. Chem. A* 2002, *106*, 5297.

28. DeMore, W. B.; Sander, S. P.; Golden, D. M.; Hampson, R. F.; Kurylo, M. J.; Howard, C. J.; Ravishankara, A. R.; Kolb, C. E.; Molina, M. J.; *Chemical Kinetics and Photochemical Data for use in Stratospheric Modeling*; Evaluation No. 12; JPL Publication 97-4; JPL: Pasadena, CA, January 15, 1997.

29. Smith, O. I.; Tseregounis, S.; Wang, S.-N.; *Int. J. Chem. Kinet.* 1982, *14*, 679.

30. Atkinson, R.; Pitts, J. N., Jr.; Int. J. Chem. Kinet. 1978, *10*, 1081.

31. Mulcahy, M. F. R.; Steven, J. R.; Ward, J. C.; *J. Phys. Chem.* 1967, *71*, 2124.

32. Troe, J.; *Ann. Rev. Phys. Chem.* 1978, *29*, 223.

33. Westenberg, A. A.; deHaas, N.; *J. Chem. Phys.* 1975, *63*, 5411.

34. Atkinson, R,; Baulch, D. L.; Cox, R. A.; Frank, P.; Hampson, R. F.; Kerr, J. A.; Rossi, M. J.; Troe, J.; *J. Phys. Chem. Ref. Data* 1997, *26*, 1329.

35. Ashtoltz, D. C.; Glanzer, K.; Troe, J.; *J. Chem. Phys.* 1979, *70*, 2409.

36. Mueller, M. A.; Yetter, R. A.; Dryer, F. L.; *Int. J. Chem. Kinet.* 2000, *32*, 317.

Appendix B

Hydroxysulfonyl (HOSO$_2$)

$\Delta_f H^0(298.15 \text{ K}) = -391.2 \text{ kJ mol}^{-1}$

Vibrational Frequencies (cm^{-1}) and Degeneracies:
3539.8 (1)
1309.2 (1)
1296.2 (1)
1097.2 (1)
 759.3 (1)
 544   (1)
 491   (1)
 437   (1)
 252   (1) – torsion

Ground State Quantum Weight: 2 (^{2}A')
Point Group: C$_1$
External Rotational Symmetry Number: $\sigma = 1$
Bond Length (angstrom):
r(S–O1)=1.612
r(S–O2)=1.444
r(S–O3)=1.436
r(O1–H)=0.967
Bond Angle (degree):
θ(S–O1–H)=107.2
θ(O1–S–O2)=108.4
θ(O1–S–O3)=106.0
τ(O2–S–O1–H)=26.1
τ(O3–S–O1–H)=161.1
Product of the Moment of Inertia: $I_x I_y I_z = 1.473 \times 10^{-114} \text{ g}^3 \text{ cm}^6$
Reduced Moment of Inertia: $I_r = 1.405 \times 10^{-40} \text{ g cm}^2$
Internal Rotational Symmetry Number: $n=2$
Barrier to Internal Rotation: $V_0 = 9.5 \text{ kJ mol}^{-1}$

Enthalpy of Formation

From Benson's estimate for $D^0_{298.15}$(HO–SO$_2$)=36±3 kcal mol^{-1},1 $\Delta_f H^0$ (298.15 K) = –409 kJ mol^{-1} (–98 kcal mol^{-1}) was derived. This value of $\Delta_f H^0$ (298.15 K) gives $\Delta_r H^0$ (298.15 K)=6 kcal mol^{-1} for the reaction, HOSO$_2$+O$_2$ → HO$_2$+ SO$_3$.

Margitan's rate coefficients measurement for the above reaction put an upper limit for the reaction endothermicity, $\Delta_r H^0$ (298.15 K)$\leq$2 kcal mol^{-1} ($D^0_{298.15}$(HO–SO2)$\leq$32 kcal mol^{-1}).[2] Gleason and Howard set a limit on the endothermicity of the reaction (1), $\Delta_r H^0$ (298.15 K)$\leq$3

$k$cal mol^{-1},[3] which places a lower limit of $\Delta_f H^0$ (298.15 K)$\geq$–395.4 kJ mol^{-1} ($\geq$–94.5 $k$cal mol^{-1}). Here we adopted Margitan's value of $\Delta_r H^0$ (298.15 K) = 2 $k$cal mol^{-1}, which gives $\Delta_f H^0$ (298.15 K)=–391.2 kJ mol^{-1} (–93.5 $k$cal mol^{-1}).

Heat Capacity and Entropy

The molecular structure of $HOSO_2$ was taken from the results of MP2 level calculation with cc-pVQZ basis set by Majumdar et al.[4] The reduced moment of inertia, I_r, for the hindered internal rotation was calculated by assuming $HOSO_2$ is essentially a *cis* form.[4] This assumption sets the internal rotational symmetry number, n=2. The rotational barrier was calculated using the equation, $2\pi c\omega/n=(V_0/2I_r)1/2$, where c is the speed of light and ω is the torsional frequency, 252 cm^{-1}.

Hashimoto et al. measured four vibrational frequencies of $HOSO_2$ in an argon matrix at 11 K.[5] Nagase et al. confirmed the four vibrational frequencies using the same method of Hashimoto et al. and also calculated the geometry and vibrational frequencies at the unrestricted HF level with the 3–21G(*) basis set.[6] Later, Kuo et al. measured vibrational frequencies of $HOSO_2$ in the argon matrix at 12 K.[7] The four frequencies reported by Hashimoto et al. and Nagase et al. were again confirmed. An additional frequency corresponding to HOS bend at 1296.2 cm^{-1} was measured.[7] Here, we took five experimental frequencies (3539.8, 1309.2, 1296.2, 1097.2, 759.3) of Hashimoto et al., Nagase et al. and Kuo et al. and four computed frequencies (544, 491, 437, 252) of Nagase et al. for the derivation of heat capacity and entropy.

References

1. Benson, S. W.; *Chem. Rev.* 1978, *78*, 23.
2. Margitan, J. J.; *J. Phys. Chem.* 1984, *88*, 3314.
3. Gleason, J. F.; Howard, C. J.; J. Phys. Chem. 1988, *92*, 3414.
4. Majumdar, D.; Kim, G.-S.; Kim, J.; Oh, K. S.; Lee, J. Y.; Choi, W. Y.; Lee, S.-H.; Kang, M.-H.; Min, B. J.; *J. Chem. Phys.* 2000, *112*, 723.
5. Hashimoto, S.; Inoue, G.; Akimoto, H.; *Chem. Phys. Lett.* 1984, *107*, 198.
6. Nagase, S.; Hashimoto, S.; Akimoto, H.; *J. Phys. Chem.* 1988, *92*, 641.
7. Kuo, Y.-P.; Cheng, B.-M.; Lee, Y.-P.; *Chem. Phys. Lett.* 1991, *177*, 195.

Hydroxysulfinyl (HOSO)

$\Delta_f H^0(0\ K) = -237.4 \pm 10\ kJ\ mol^{-1}$

Vibrational Frequencies (cm^{-1}) and Degeneracies:
3476 (1)
1351 (1)
1073 (1)
764 (1)
343 (1)
200 (1) – torsion

Ground State Quantum Weight: 2 ($^2A''$)
Point Group: C_s
External Rotational Symmetry Number: $\sigma = 1$
Bond Length (angstrom):
r(S–O1)=1.661
r(S–O2)=1.482
r(O1–H)=0.983
Bond Angle (degree):
θ(S–O1–H)=106.9
θ(O1–S–O2)=109.8
Product of the Moment of Inertia: $I_x I_y I_z = 2.539 \times 10^{-115}\ g^3\ cm^6$
Reduced Moment of Inertia: $I_r = 1.585 \times 10^{-40}\ g\ cm^2$
Internal Rotational Symmetry Number: n=2
Barrier to Internal Rotation: $V_0 = 7.9\ kJ\ mol^{-1}$

Enthalpy of Formation, Heat Capacity and Entropy

The enthalpy of formation of HOSO and its geometry and vibrational frequencies have not been measured experimentally. The most reliable information is from theoretical calculations of Laakso et al.[1] Laakso et al. optimized geometry and vibrational frequencies at the MP2=FULL/6–31G* level. Energies were obtained with G2 theory. For the enthalpy of formation, the changes in G2 energy for the reaction, HOSO $\rightarrow$ OH+SO ($\Delta_r H^0(0\ K)$=280.8 kJ mol^{-1}) was obtained and then $\Delta_f H^0(0\ K)$ of HOSO was derived using the measured $\Delta_f H^0(0\ K)$ values of OH and SO in the JANAF tables.[2] Laakso et al. proved the reliability of their calculation by comparing their G2 level $\Delta_r H^0(0\ K)$ for the reaction, HS+O$_2$ $\rightarrow$ OH+SO with that of the experimental value from the JANAF tables. Only a small difference in the reaction enthalpy, $\Delta_r H^0\ (0\ K)$= 0.3 kJ mol^{-1} resulted. However, a recent measurement and quantum calculation of D^0(OH, 0 K)[3,4] gave $\Delta_f H^0$ (OH, 0 K)=8.85$\pm$0.07 kcal mol^{-1} (37.03$\pm$0.29 kJ mol^-^{1}). Thus the calculated $\Delta_r H^0(0\ K)$ value for HS+O$_2$ $\rightarrow$ OH+SO reaction by Laakso et al. would be different from 0.3 kJ mol^{-1}. Since D^0(0 K) for HOSO dissociation from Laakso et al. is the only available value, we adopted this value and calculated the enthalpy of formation of HOSO using the newly measured $\Delta_f H^0$ of OH and NASA value of SO at 0 K. The recommended enthalpy of formation of HOSO is $\Delta_f H^0$ (HOSO, 0 K)=$\Delta_f H^0$(OH, 0 K)+$\Delta_f H^0$(SO, 0 K)–

$279.2 = 37.03 + 4.7143 - 279.2 \ kJ \ mol^{-1} = -237.4 \pm 10 \ kJ \ mol^{-1}$ ($-56.7 \pm 2.4 \ kcal \ mol^{-1}$) with an error bound given by Laakso et al.

For the derivation of heat capacity and entropy we took the molecular geometry and vibrational frequencies of Laakso et al. The barrier to internal rotation ($V_0 = 7.9 \ kJ \ mol^{-1}$) was directly taken from Laakso et al.'s computed G2 barrier for *cis* to *trans* transition of HOSO.

References

1. Laakso, D.; Smith, C. E.; Goumri, A.; Rocha, J.-D. R.; Marshall, P.; *Chem. Phys. Lett.* 1994, *227*, 377.
2. Chase, M. W., Jr.; Davis, C. A.; Downey, J. R.; Frurip, D. J.; McDonald, R. A.; Syverud, A. N.; *J. Phys. Chem. Ref. Data* 1985, *14*, Suppl. 1.
3. Ruscic, B.; Feller, D.; Dixon, D. A.; Peterson, K. A.; Harding, L. B.; Asher, R. L.; Wagner, A. F.; *J. Phys. Chem. A* 2001, *105*, 1.
4. Ruscic, B.; Wagner, A. F.; Harding, L. B.; Asher, R. L.; Feller, D.; Dixon, D. A.; Peterson, K. A.; Song, Y.; Qian, X.; Ng, C.-Y.; Liu, J.; Chen, W.; Schwenke, D. W.; *J. Phys. Chem. A* 2002, *106*, 2727.

Sulfinyl (HSO₂)

$\Delta_f H^0$ (298.15 K) = $-178.2 \pm 8.4 \ kJ \ mol^{-1}$

Vibrational Frequencies (cm^{-1}) and Degeneracies:
2269 (1)
1600 (1)
1128 (1)
1065 (1)
810 (1)
431 (1)

Ground State Quantum Weight: 2 ($^2A'$)
Point Group: C_s
External Rotational Symmetry Number: $\sigma = 1$
Bond Length (angstrom):
r(S–O1)=1.447
r(S–O2)=1.447
r(H–O2)=1.381
Bond Angle (degree):
θ(O1–S–O2)=123.2
θ(H–S–O2)=105.6
τ(H–S–O2(O1))=121.1

Product of the Moment of Inertia: $I_x I_y I_z = 1.485 \times 10^{-115} \ g^3 \ cm^6$

Enthalpy of Formation

Benson's estimate for the enthalpy of formation of HSO_2 was $\Delta_f H^0(298.15\ K) = -177.4 \pm 16.7\ kJ$ mol^{-1} ($-42.4 \pm 4\ kcal\ mol^{-1}$). The corresponding $D^0_{298.15}(H-SO2) = 41\ kcal\ mol^{-1}$ was compatible with the fast rate coefficients measured in flame studies at T>1600 K for the three-body recombination reaction ($H+SO_2+M=HSO_2+M$).[1] Boyd et al. performed ab initio calculations for HSO_2 at the HF/STO–3G* level.[2] Using the calculated $D^0_0(H-SO_2) = 142.1\ kJ\ mol^{-1}$ and the $\Delta_f H^0(0\ K)$ values of H and SO_2 in the JANAF tables,[3] $\Delta_f H^0(0\ K) = -220.4\ kJ\ mol^{-1}$ ($-52.7\ kcal$ mol^{-1}) was derived for HSO_2. Laakso et al. optimized geometry and vibrational frequencies for HSO_2 at the MP2=FULL/6–31G* level.[4] Energies were obtained with G2 theory. For the enthalpy of formation, the change in G2 energy for the reaction, $HSO_2 \rightarrow H+SO_2$ ($\Delta_r H^0(0$ $K) = 56.8 \pm 10\ kJ\ mol^{-1}$) was obtained and then $\Delta_f H^0(0\ K)$ of HSO_2 was derived using the measured $\Delta_f H^0(0\ K)$ values of H and SO_2 in the JANAF tables. $\Delta_f H^0(298.15\ K)$ of $HSO_2 = -141.4 \pm 10\ kJ\ mol^{-1}$($-33.8 \pm 2.4\ kcal\ mol^{-1}$) was recommended. Laakso et al. proved the reliability of their calculation by comparing their G2 level $\Delta_r H^0(0\ K)$ for the reaction, $HS+O_2 \rightarrow$ $H+SO_2$ with that of the experimental value from the JANAF tables. Considering the error limit in the G2 $\Delta_r H^0(0\ K)$ value, the difference in the reaction enthalpy, $\Delta_r H^0(0\ K) = 9.4\ kJ\ mol^{-1}$ was considered excellent. Recently, Denis and Ventura investigated the enthalpy of formation of XSO_2, X=H, CH_3 using the B3LYP and B3PW91 methods with very large basis sets up to cc–pV6Z.[5] The enthalpy of formation of HSO_2, $\Delta_f H^0(298.15\ K) = -178.2 \pm 8.4\ kJ\ mol^{-1}$ (-42.6 ± 2 $kcal\ mol^{-1}$) resulting from B3PW91 method was recommended. We adopted the enthalpy of formation of Denis and Ventura, $\Delta_f H^0(298.15\ K) = -178.2 \pm 8.4\ kJ\ mol^{-1}$ for HSO_2.

Heat Capacity and Entropy

Vibrational frequencies of HSO_2 have not been measured experimentally and only one theoretical calculation is available. For the derivation of heat capacity and entropy we used the vibrational frequencies calculated at the MP2=FULL/6–31G* level by Laakso et al.[4] The molecular geometry was taken from the theoretical calculation using the B3PW91 method with cc–pV6Z basis set by Denis and Ventura.[5]

References

1.   Benson, S. W.; *Chem. Rev.* 1978, *78*, 23.
2.   Boyd, R.; Gupta, A.; Langler, R. F.; Lownie, S. P.; Pincock, J.; *Can. J. Chem.* 1980, *58*, 331.
3.   Chase, M. W., Jr.; Davis, C. A.; Downey, J. R.; Frurip, D. J.; McDonald, R. A.; Syverud, A. N.; *J. Phys. Chem. Ref. Data* 1985, *14*, Suppl. 1.
4.   Laakso, D.; Smith, C. E.; Goumri, A.; Rocha, J.-D. R.; Marshall, P.; *Chem. Phys. Lett.* 1994, *227*, 377.
5.   Denis, P. A.; Ventura, O.; *Chem. Phys. Lett.* 2001, *344*, 221.

Mercapto (SH)

$\Delta_f H^0$(0 K)=133.03 kJ mol^{-1}

Enthalpy of Formation

The current JANAF recommendations for $\Delta_f H^0$(0 K)=136.49±5.0 kJ mol^{-1} and $\Delta_f H^0$(298.15 K)=139.33±5.0 kJ mol^{-1} are based on the measurements of HS ionization potential and the appearance potential of HS$^+$ from photoionization of H_2S.[1] The previous NASA recommendation for $\Delta_f H^0$(298.15 K)[2] was also 139.33 kJ mol^{-1}. Continetti and Lee[3] performed photodissociation of H_2S at 193.3 nm using H-atom photofragment-translational spectroscopy with mass spectroscopic detection. They found D^0_0(H–S)=349.27±2.89 kJ mol^{-1} (83.48±0.69 $kcal$ mol^{-1}) in the secondary photodissociation of HS radicals, formed in the primary H_2S photodissociation experiments. Nicovitch et al.[4] measured the forward and reverse reaction rate coefficients of Br($^2P_{3/2}$)+H_2S=HS+HBr over the temperature range of 319 to 431 K. Using both the "second law method" and the "third law method," an average value of $\Delta_r H^0$ at a given temperature was obtained, then the values of $\Delta_r H$(0 K) and $\Delta_r H^0$(298.15 K) were calculated by applying heat capacity corrections from data in JANAF tables for Br, H_2S, HS and HBr. The reported values for the enthalpy of formation and the bond dissociation energy are $\Delta_f H^0$(0 K)=142.55±3.01 kJ mol^{-1} (34.07±0.72 $kcal$ mol^{-1}), $\Delta_f H^0$(298.15 K)=143.01±2.85 kJ mol^{-1} (34.18±0.68 $kcal$ mol^{-1}) and D^0_0(H–S)=348.23±3.26 kJ mol^{-1}(83.23±0.78 $kcal$ mol^{-1}), $D^0$298.15(H–S)=351.96±3.10 kJ mol^{-1} (84.12±0.74 $kcal$ mol^{-1}), respectively. We adopted the bond dissociation energy of Continetti and Lee, D^0_0(H–S)=349.27±2.89 kJ mol^{-1} (83.48±0.69 $kcal$ mol^{-1}) and derived $\Delta_f H^0$(0 K)=$\Delta_f H^0_0$(S)+$\Delta_f H^0_0$(H)–349.27=270.5126+211.8014–349.27=133.03 kJ mol^{-1} (31.80 $kcal$ mol^{-1}).

References

1.   Chase, M. W., Jr.; Davis, C. A.; Downey, J. R.; Frurip, D. J.; McDonald, R. A.; Syverud, A. N.; *J. Phys. Chem. Ref. Data* 1985, *14*, Suppl. 1.
2.   Mcbride, B. J.; Gordon, S.; Reno, N. A.; *Coefficients for Calculating Thermodynamic and Transport Properties of Individual Species*; NASA TM-4513; NASA: Washington, DC, 1993.
3.   Continetti, R. E.; Balko, B. A.; Lee, Y. T.; *Chem. Phys. Lett.* 1991, *182*, 400.
4.   Nicovich, J. M.; Kreutter, K. D.; van Dijk, C. A.; Wine, P. H.; *J. Phys. Chem.* 1992, *96*, 2518.

Hydrogen Sulfur Oxide (HSO)

$\Delta_f H^0$(0 K)=–3.8 kJ mol^{-1}

Vibrational Frequencies (cm^{-1}) and Degeneracies:
2480 (1)
1164 (1)
1026 (1)

Ground State Quantum Weight: 2 (2A'')
Point Group: C1
External Rotational Symmetry Number: s=1
Bond Length (angstrom):
r(S–O)=1.494
r(S–H)=1.389
Bond Angle (degree):
θ (H–S–O)=106.6
Product of the Moment of Inertia: $I_x I_y I_z$=5.028×10^{-117} g^3 cm^6

Enthalpy of Formation

Schurath et al.[1] measured the chemiluminescence spectrum of the X^2A'' ← A^2A' transition of HSO and DSO. The $\Delta_r H^0$(298.15 K) for the reaction HS+O$_3$ → HSO+O$_2$ (HS+O$_3$ → HSO*+O$_2$, HSO* → HSO) was estimated using the observed highest level of HS–O vibration, v '$_3$=7, which corresponds to 19149 cm^{-1} (54.74 kcal mol^{-1}). Using $-\Delta_r H^0$(298.15 K)≤54.74 kcal mol^{-1} and the values of the enthalpy of formation of HS and O$_3$ available, Schurath et al.[1] set an upper limit of $\Delta_f H^0$(298.15 K)≤14.9 kcal mol^{-1}. White and Gardiner[2] reanalyzed the results of Schurath et al. and presented 12.2 $\Delta_f H^0$(298.15 K)<14.1 kcal mol^{-1}. Benson's estimate[3] was $\Delta_f H^0$(298.15 K)=–5±4 kcal mol^{-1} Slagle et al.[4] suggested $\Delta_f H^0$ (298.15 K)=–3 kcal mol^{-1}, based upon their kinetic work on the reaction O(^{3}P)+H$_2$S → HSO+H. Davidson et al.[5] studied the reactive scattering of O atoms with H$_2$S molecules using a crossed molecular beam mass spectrometric detection of HSO radicals. The value of the enthalpy of formation obtained was $\Delta_f H^0$(298.15 K)=–1.4±1.9 kcal mol^{-1} (–6±8 kJ mol^{-1}). Balucani et al.[6] determined $\Delta_f H^0$(0 K) =–0.9±0.7 kcal mol^{-1} (–3.8±2.9 kJ mol^{-1}) from the analysis of high resolution crossed beam reactive scattering experiments on the reaction O(^{3}P)+H$_2$S → HSO+H. Here we took Balucani et al.'s value $\Delta_f H^0$(0 K)=–0.9±0.7 kcal mol^{-1} (–3.8±2.9 kJ mol^{-1}).

Heat Capacity and Entropy

The molecular geometries and vibrational frequencies of HSO and DSO radicals were determined by Schurath et al.,[1] Kakimoto et al.,[7] and Ohashi et al.[8] Following the measurements of Schurath et al., Kakimoto et al. and Ohashi et al. observed the doppler-limited dye laser excitation spectra of the A^2A'(003)← X^2A''(000) vibronic transition of HSO and DSO. Here we took the structural parameters of HSO from those of Ohashi et al. and Kakimoto et al., instead of the "best fit" values used in vibronic band contour synthesis by Schurath et al. The product of moment of inertia, $I_x I_y I_z$, was calculated using the directly measured rotational constants, B_x, B_y, and B_z of Ohashi et al.

The three ground state ($^2A''$) vibrational frequencies, H–SO stretching (ω_1), H–S–O bending (ω_2), and HS–O stretching (ω_3), were presented by Schurath et al.[1] From v '$_3$ progression, ω_3 (1013 cm^{-1}) was measured. The quantity ω_2 was estimated (1063 cm^{-1}) using the measured bending frequency of DSO and the isotope factor. For ω_1, the recommended—S–H group frequency (2570 cm^{-1})[9] was assigned. However, the harmonic force field analysis by Ohashi et al.[8] yielded ω_2=1164 cm^{-1} and ω_3=1026 cm^{-1}. The force constant, k_1, was estimated by applying

Badger's rule using the bond lengths and force constants of $HS(^2\Pi)$ and $HS(^2\Sigma^+)$ as references. From this estimated force constant $\omega_1 = 2271$ cm^{-1} was calculated.

Here we adopted $\omega_2 = 1164$ cm^{-1} and $\omega_3 = 1026$ cm^{-1} of Ohashi et al. We believe the ω_1 value from—S–H group frequency is too high and that of Ohashi et al. is too low. Therefore we estimated the ω_1 value in the following manner: Using the known H–O and H–OO stretching frequencies the force constant change from H–O to H–OO was calculated. For H–OO stretching the force constant was reduced by 15% from that of H–O. Since HS and HSO are isovalent radicals of HO and HOO, respectively, we calculated the force constant of H–SO by applying the same 15% reduction to the H–S force constant. The ω_1 value was calculated to be $\omega_1 = (1/2\pi c)(k_1/m_H)^{1/2} = 2480$ cm^{-1}, where c is the speed of light and m_H is the mass of the terminal H atom.

References

1.   Schurath, U.; Weber, M.; Becker, K. H.; *J. Chem. Phys.* 1977, *67*, 110.
2.   White, J. N.; Gardiner, W. C., Jr.; *Chem. Phys. Lett.* 1978, *58*, 470.
3.   Benson, S. W.; *Chem. Rev.* 1978, *78*, 23.
4.   Slagle, I. R.; Baiocchi, F.; Gutman, D.; *J. Phys. Chem.* 1978, *82*, 1333.
5.   Davidson, F. E.; Clemo, A. R.; Duncan, G. L.; Browett, R. J.; Hobson, J. H.; Grice, R.; *Mol. Phys.* 1982, *46*, 33.
6.   Balucani, N.; Casavecchia, P.; Stranges, D.; Volpi, G. G.; *Chem. Phys. Lett.* 1993, *211*, 469.
7.   Kakimoto, M.; Saito, S.; Hirota, E. J.; *Mol. Spectrosc.* 1980, *80*, 334.
8.   Ohashi, N.; Kakimoto, M.; Saito, S.; Hirota, E. J.; *Mol. Spectrosc.* 1980, *84*, 204
9.   Herzberg, G.; *Molecular Spectra and Molecular Structure II. Infrared and Raman Spectra of Polyatomic Molecules*; Van Nostrand: New York, 1945.

REPORT DOCUMENTATION PAGE

Public reporting burden for this collection of information is estimated to average 1 hour per response, including the time for reviewing instructions, searching existing data sources, gathering and maintaining the data needed, and completing and reviewing the collection of information. Send comments regarding this burden estimate or any other aspect of this collection of information, including suggestions for reducing this burden, to Washington Headquarters Services, Directorate for Information Operations and Reports, 1215 Jefferson Davis Highway, Suite 1204, Arlington, VA 22202-4302, and to the Office of Management and Budget, Paperwork Reduction Project (0704-0188), Washington, DC 20503.

1. AGENCY USE ONLY (Leave blank)	2. REPORT DATE April 2003	3. REPORT TYPE AND DATES COVERED Annual Contractor Report

4. TITLE AND SUBTITLE

Sulfur Oxidation and Contrail Precursor Chemistry

5. FUNDING NUMBERS

WU–708–87–23–00
NAG3–2674

6. AUTHOR(S)

Kenneth J. De Witt

7. PERFORMING ORGANIZATION NAME(S) AND ADDRESS(ES)

University of Toledo
Department of Chemical Engineering
2801 W. Bancroft St.
Toledo, Ohio 43606

8. PERFORMING ORGANIZATION REPORT NUMBER

E–13855

9. SPONSORING/MONITORING AGENCY NAME(S) AND ADDRESS(ES)

National Aeronautics and Space Administration
Washington, DC 20546–0001

10. SPONSORING/MONITORING AGENCY REPORT NUMBER

NASA CR—2003-212293

11. SUPPLEMENTARY NOTES

12a. DISTRIBUTION/AVAILABILITY STATEMENT

Unclassified - Unlimited
Subject Categories: 01 and 07   Distribution: Nonstandard

Available electronically at http://gltrs.grc.nasa.gov

This publication is available from the NASA Center for AeroSpace Information, 301–621–0390.

12b. DISTRIBUTION CODE

13. ABSTRACT (Maximum 200 words)

Sulfuric acid (H_2SO_4), formed in commercial aircraft operations via fuel—S $\rightarrow$ SO_2 $\rightarrow$ SO_3 $\rightarrow$ H_2SO_4, plays an important role in the formation of contrails. It is believed that the first step occurs inside the combustor, the second step in the engine exit nozzle, and the third step in the exhaust plume. Thus, measurements of the sulfur oxidation rates are critical to the understanding of contrail formation. Field measurements of contrails formed behind commercial aircraft indicate that significantly greater conversion of fuel-bound sulfur to sulfate aerosol occurs than can be explained by our current knowledge of contrail physics and chemistry. The conversion of sulfur from S(IV) to S(VI) oxidation state, required for sulfate aerosol formation, is thermodynamically favored for the conditions that exist within jet engines but is kinetically disfavored. The principal reaction pathway is $O+SO_2+M \rightarrow SO_3+M$. The rates of this reaction have never been measured in the temperature and pressure regimes available to aircraft operation. In the first year (FY02) of this project, we performed a series of experiments to elucidate the rate information for the $O+SO_2+M \rightarrow SO_3+M$ reaction. The work performed is described below, following the proposed work plan. Because we used the H_2/O_2 system for an O-atom source and rate coefficients were obtained via computer simulation, construction of a reaction mechanism and either recalculation or estimation of thermodynamic properties of H_xSO_y species are described first.

14. SUBJECT TERMS

Sulfur oxidation; Contrail formation

15. NUMBER OF PAGES

34

16. PRICE CODE

17. SECURITY CLASSIFICATION OF REPORT	18. SECURITY CLASSIFICATION OF THIS PAGE	19. SECURITY CLASSIFICATION OF ABSTRACT	20. LIMITATION OF ABSTRACT
Unclassified	Unclassified	Unclassified	